Journal of Catalysis **209,** 35–42 (2002)
doi:10.1006/jcat.2002.3620

The Relationship between the Electronic and Redox Properties of Dispersed Metal Oxides and Their Turnover Rates in Oxidative Dehydrogenation Reactions

Kaidong Chen, Alexis T. Bell,[1] and Enrique Iglesia[1]

Chemical Sciences Division, Lawrence Berkeley National Laboratory, and Department of Chemical Engineering, University of California, Berkeley, California 94720-1462

Received August 29, 2001; revised February 11, 2002; accepted March 24, 2002

The mechanistic connections among propane oxidative dehydrogenation (ODH) rates, H_2 reduction rates, and the electronic transitions responsible for the absorption edge in the electronic spectra of dispersed metal oxides were explored for VO_x, MoO_x, WO_x, and NbO_x samples consisting predominately of two-dimensional oxide domains supported on Al_2O_3, ZrO_2, and MgO. For a given active oxide, propane turnover rates increased in parallel with the reduction rate of the oxide catalyst using H_2, but propane ODH rates differed significantly among different metal oxide samples with similar H_2 reduction rates. For all catalysts, ODH turnover rates increased monotonically as the energy of the absorption edge in the UV–visible spectrum decreased. These results, taken together with the respective mechanisms for electron transfer during C–H bond activation and during the ligand-to-metal charge-transfer processes responsible for the UV–visible edge, suggest that the stability of activated complexes in C–H bond dissociation steps depends sensitively on the ability of the active oxide domains to transfer electrons from lattice oxygen atoms to metal centers. The electronic transitions responsible for the UV–visible absorption edge are mechanistically related to the redox cycles involving lattice oxygens responsible for oxidative dehydrogenation turnovers of alkanes. As a result, the details of near-edge electronic spectra provide useful guidance about intrinsic reaction rates on active oxides typically used for these reactions.

INTRODUCTION

The oxidative dehydrogenation (ODH) of propane provides a low-temperature route for the synthesis of propene (1–14). Catalyst compositions based on V and Mo oxides have shown attractive ODH rates and propene selectivities (3). Several studies have probed primary and secondary reactions responsible for the observed selectivity during propane ODH reactions (1–3, 9–14). The kinetically relevant steps for both propane dehydrogenation and combustion reactions involve the activation of methylene C–H bonds in propane (9). Detailed reaction kinetics and mechanistic studies have shown that C–H bond activation steps involve lattice oxygen atoms and that each reaction turnover requires a two-electron reduction of high-valent M^{+n} cations to form one M^{n-2} or two M^{n-1} cations (9–11); as a result of these cycles, the redox properties of oxides influence their ability to catalyze such reaction turnovers. On VO_x- and MoO_x-based catalysts, the rate constants for reoxidation of reduced centers using O_2 are greater than for their re-reduction by C–H bond activation steps. Several studies (1–3, 14–21) have proposed that alkane ODH rates increase as active metal oxides become more reducible, without providing a rigorous definition of reducibility or an appropriate method to measure it. The reduction peak temperatures during reduction of oxides in H_2 (14–23), generally used as a measure of reducibility, reflect instead the nucleation and growth of a new crystal structure during a stoichiometric reduction, and not merely the formation of a few reduced centers in a structurally intact stoichiometric oxide. In addition, the mechanism of reduction using H_2 may differ from the related processes using propane as the reductant, and the measured ODH reaction rates can reflect a complex interplay between site reactivity and the surface accessibility of oxide structures, which are seldom atomically dispersed.

Here, we explore the electron transfer processes required for C–H bond activation steps and the factors responsible for the redox processes involved in each propane turnover. Propane ODH turnover rates are reported on active oxides (VO_x, MoO_x, NbO_x, and WO_x) dispersed as isolated or two-dimensional species on the surface of inactive supports. These turnover rates are related to those for the incipient formation of vacancies during the stoichiometric reduction of the oxides using H_2 and to the energy required for the ligand-to-metal electron transfer processes responsible for the edge energy in the UV–visible absorption spectrum. A decrease in the energy required for local photoreduction events occurring during this electron transfer was accompanied by a faster C–H bond activation step during

[1] To whom correspondence should be addressed. E-mail: iglesia@cchem.berkeley.edu; bell@cchem.berkeley.edu.

0021-9517/02 $35.00

propane ODH. Facile electron transfer between occupied orbitals in lattice oxygen and empty states in the metal centers leads to more stable activated complexes in the kinetically relevant elementary chemical steps for propane ODH and to lower required photon energies for electron promotion between these two energy levels.

EXPERIMENTAL METHODS

Al_2O_3, ZrO_2, or MgO were used as inactive supports for V_2O_5, MoO_3, WO_3, or Nb_2O_5 species predominately present as isolated or two-dimensional structures. Samples were prepared by incipient wetness impregnation of γ-Al_2O_3, $ZrO_x(OH)_{4-2x}$, or MgO with a solution of ammonium vanadate (12, 13, 26), ammonium heptamolybdate (14), ammonium metatungstate (24, 25), or ammonium niobium oxalate (27). Impregnated samples were dried overnight in ambient air at 393 K and then treated in flowing dry air at 773 K for 3 h. Surface areas were measured by N_2 physisorption at its normal boiling point using a Quantasorb surface-area analyzer (Quantachrome Corporation) and standard BET analysis methods.

The rates of stoichiometric reduction of these dispersed metal oxides using H_2 were measured using a Quantasorb surface-area analyzer (Quantachrome Corporation) modified with electronic mass-flow controllers. Samples were heated in 20% H_2/Ar (1.33 $cm^3\ s^{-1}$; Matheson UHP, certified mixture) at 0.167 K s^{-1} to 1200 K. H_2 concentrations were measured using a thermal conductivity detector after removing the water formed during reduction using a 13× molecular sieve trap held at ambient temperature. The detector response was calibrated using the reduction of CuO powder (Aldrich, 99.995%). The samples were held within a quartz cell (4 mm I.D.) containing a quartz thermowell in contact with the sample bed. The amount of catalyst was varied in order to maintain a constant number of metal atoms in all experiments (space velocities, 0.22 mol H_2/g-atom V s^{-1} and 0.34 mol H_2/g-atom Mo s^{-1}). The very initial stages of reduction (oxygen conversion, <10%) were analyzed by fitting the reduction rate data using an Arrhenius dependence in order to obtain a rate constant as a function of temperature for these low extents of reduction.

Diffuse reflectance UV–visible spectra were obtained using a Varian–Cary 4 spectrophotometer equipped with a Harrick diffuse-reflectance attachment and an *in situ* reaction chamber. MgO (Mallinckrodt, AR) powders were used as a reference. Reflectance measurements were converted to absorption spectra using the Kubelka–Munk function (28). UV–visible spectra were measured in the 1.5- to 5.0-eV photon energy range.

Propane oxidative dehydrogenation rates and selectivities were measured at 703 K using a packed-bed tubular quartz reactor and 0.01- to 0.3-g catalyst samples. Propane (14 kPa; Airgas, 99.9%) and oxygen (1.7 kPa; Airgas, 99.999%) diluted with He (Airgas, 99.999%) were used as reactants. Reactants and products were analyzed by gas chromatography (Hewlett–Packard 5890 GC) using procedures described previously (12, 13). C_3H_8 and O_2 conversions were varied by changing reactant space velocities (F/w; w, catalyst mass; F, reactant volumetric flow rate). Reactant conversions were <2% for C_3H_8 and <20% for O_2. Initial propane turnover rates and selectivities were obtained by extrapolation of these data to zero residence time using reaction rate data obtained over a wide range of space velocities. Rates and rate constants for secondary propene combustion reactions were calculated from the corresponding effects of bed residence time on product selectivity, using procedures reported previously (12, 13).

RESULTS AND DISCUSSION

Surface areas and MO_x surface densities (M = V, Mo, W, or Nb) are shown in Table 1 for all samples. These samples were characterized by X-ray diffraction and by X-ray absorption, Raman, and UV–visible spectroscopies. The details of these measurements have been reported previously (12–14, 24–27). These methods showed that the active oxide species at these surface densities consist predominately of two-dimensional oligomeric domains. These two-dimensional structures expose most MO_x structures at surfaces, where they can be used for catalytic reaction turnovers. Thus, reaction rates normalized by the number of metal atoms in each sample become turnover rates, as a

TABLE 1

Structure Characterization Results of Supported MO_x Catalysts[a]

Catalyst	BET surface area (m^2/g)	MO_x surface density[a] (M/nm^2)	Predominant MO_x structure[a,b]
0.7 wt% V_2O_5/Al_2O_3	88	0.5	Monovanadate
2 wt% V_2O_5/Al_2O_3	100	1.3	Polyvanadate
5 wt% V_2O_5/Al_2O_3	96	3.2	Polyvanadate
10 wt% V_2O_5/Al_2O_3	86	7.7	Polyvanadate
2 wt% V_2O_5/ZrO_2	144	0.9	Polyvanadate
5 wt% V_2O_5/ZrO_2	155	2.1	Polyvanadate
10 wt% V_2O_5/ZrO_2	170	3.9	Polyvanadate
15 wt% V_2O_5/ZrO_2	160	6.2	Polyvanadate
5 wt% V_2O_5/MgO	307	1.1	Monovanadate
2 wt% MoO_3/Al_2O_3	99	0.8	Polymolybdate
4 wt% MoO_3/Al_2O_3	107	1.6	Polymolybdate
6 wt% MoO_3/Al_2O_3	100	2.5	Polymolybdate
8 wt% MoO_3/Al_2O_3	99	3.4	Polymolybdate
10 wt% MoO_3/Al_2O_3	94	4.4	Polymolybdate
2 wt% WO_3/ZrO_2	124	4.2	Polytungstate
5 wt% Nb_2O_5/Al_2O_3	105	2.8	Polyniobate
10 wt% Nb_2O_5/Al_2O_3	105	5.6	Polyniobate

[a] M = V, Mo, W, Nb.
[b] Inferred from XAS, Raman, and UV–visible spectroscopy data.

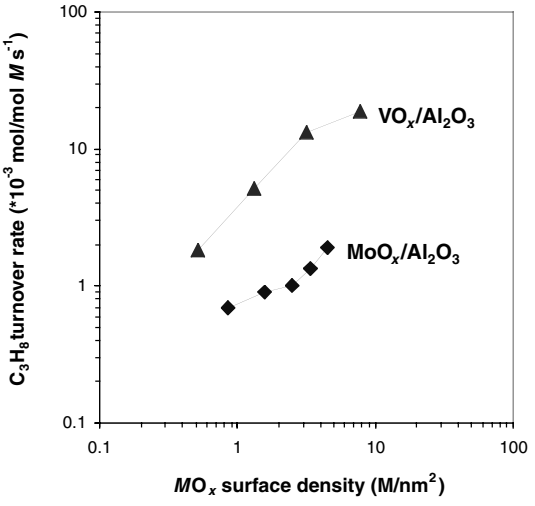

FIG. 1. Dependence of propane turnover rate (703 K, 14 kPa C_3H_8, 1.7 kPa O_2, balance He) on the MO_x surface density.

result of the effective access of reactants to all MO_x species. Catalysts with bulk MO_x clusters (detected by Raman or X-ray diffraction) are not included in this study, but details of their catalytic and structural properties can be found in previous studies (12–15, 24–27).

Propane oxidative dehydrogenation turnover rates are shown in Fig. 1 as a function of MO_x surface density for VO_x and MoO_x species supported on Al_2O_3. On both types of samples, turnover rates increased with increasing MO_x surface density. At a given MO_x surface density, turnover rates are greater on VO_x than on MoO_x samples, suggesting that the redox cycles required for each ODH turnover occur more rapidly on VO_x domains than on MoO_x domains of similar size. These differences are consistent with the higher ODH reaction temperatures reported on Mo-based compared with V-based catalysts (3).

Previous studies have suggested that the higher ODH rates observed on VO_x species reflect their more reducible nature compared with that of MoO_x species (14–21). These studies, however, were not restricted to well-dispersed oxides with completely accessible active oxides; thus, reported reaction rates did not reflect the true activity of sites exposed at the surface of MO_x domains. Also, reduction kinetics were not rigorously measured and the reducibility was inferred solely from the temperature of one or more of the observed reduction peaks. These reduction peaks reflect the structural transformation of the starting high-valent oxides into structurally distinct suboxides, instead of merely the ease of removal of the few oxygen atoms (<5%) generally missing during steady-state ODH reactions (9–11).

Next, we report the reduction kinetics of VO_x and MoO_x catalysts measured during the initial stages of reduction in H_2. Figure 2 shows H_2 consumption rates as a function of temperature during the reduction of VO_x/Al_2O_3 and MoO_x/Al_2O_3. Figure 2 shows that the reduction peak maxima shift to lower temperature as the surface density of the active oxides increases in VO_x and MoO_x samples. This peak temperature occurs, however, at an extent of reduction requiring significant restructuring to form distinct suboxides, as detected by evolution of X-ray diffraction and absorption features from those of MoO_3 to MoO_2 and ultimately to Mo metal as reduction proceeds. Figure 3 shows H_2 consumption rates at 673 K (obtained using the method described in the experimental section) as a function of MO_x surface density. H_2 reduction rates are reported at 673 K because this temperature leads to low extents of reduction (5–10% of total V^{5+} or Mo^{6+}), which resemble the anticipated density of oxygen vacancies during steady-state ODH reactions at the conditions of our ODH rate measurements

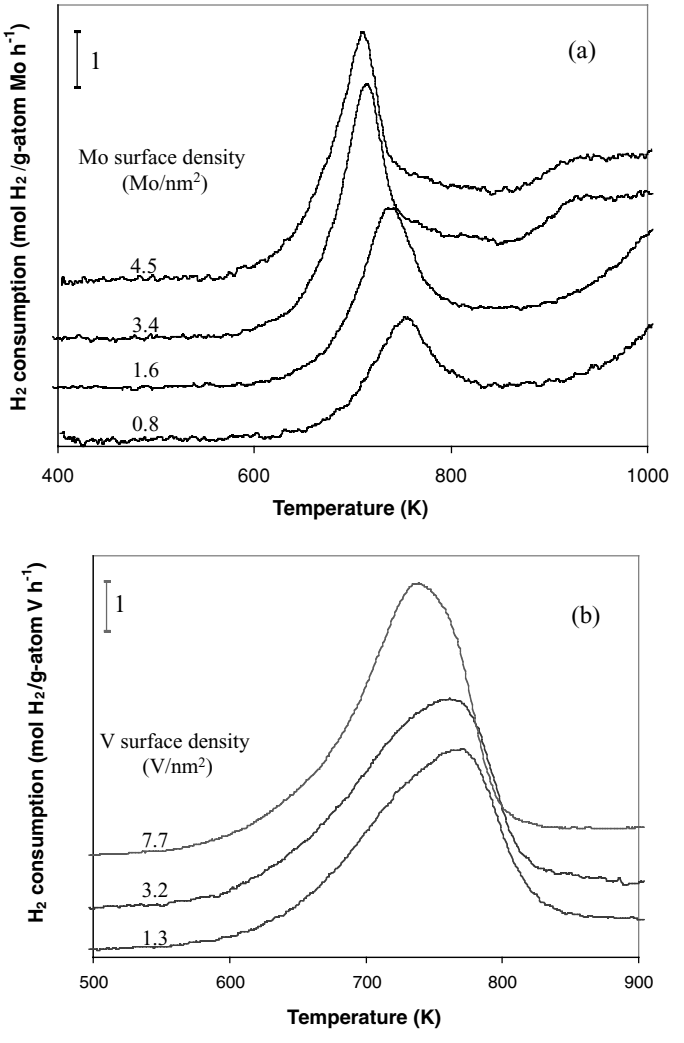

FIG. 2. Temperature-programmed reduction profiles of (a) MoO_x/Al_2O_3 and (b) VO_x/Al_2O_3 catalysts (5 mg MoO_3 or V_2O_5, 20% H_2/Ar, 0.167 K s^{-1}).

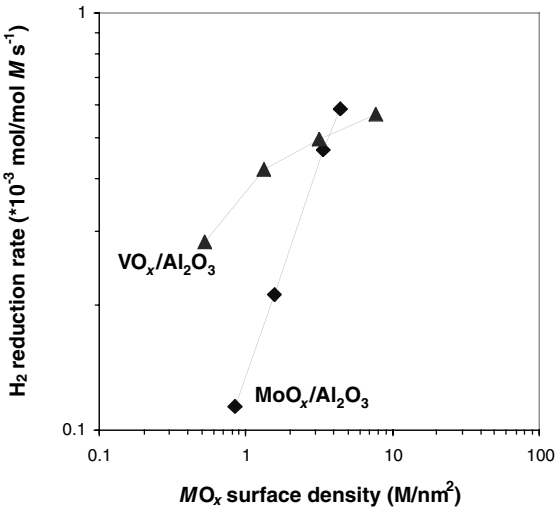

FIG. 3. Dependence of H_2 reduction rate (5 mg MoO_3 or V_2O_5, 20% H_2/Ar, 673 K) on the MO_x surface density.

(29). H_2 reduction rates at 673 K increase with increasing MO_x surface density (Fig. 3), in parallel with the observed increase in ODH turnover rates (Fig. 1).

Figure 4 shows propane ODH turnover rates and initial rates of reduction in H_2 (from the data in Fig. 3) for VO_x and MoO_x domains supported on alumina. A parallel increase in these rates is apparent for each active oxide, but ODH turnover rates on VO_x catalysts are significantly higher than on MoO_x catalysts, even at similar values of the measured H_2 reduction rates. This suggests that differences in structural or chemical properties of VO_x and MoO_x domains are

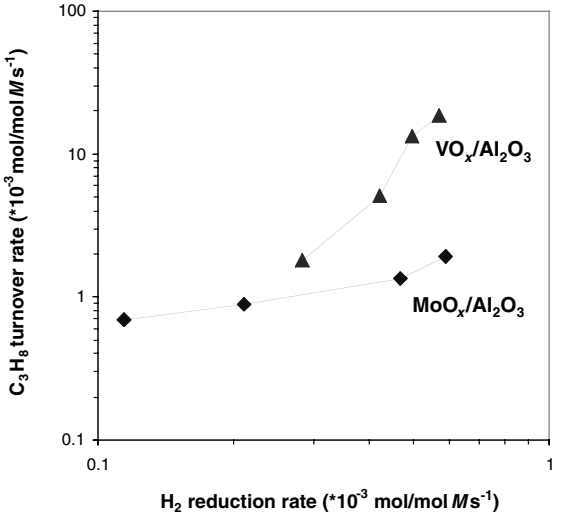

FIG. 4. Dependence of propane turnover rate (703 K, 14 kPa C_3H_8, 1.7 kPa O_2, balance He) on H_2 reduction rate (5 mg MoO_3 or V_2O_5, 20% H_2/Ar, 673 K) for MO_x catalysts.

"felt" differently by the two reactions, and that their correlation is incomplete without the detection and assessment of such differences. Clearly, the structural and chemical requirements for ODH and H_2 reduction processes are shared only to some extent. The rate of reduction in H_2 may well be appropriate as a complete description of the processes required for a propane turnover for a given metal oxide, as suggested by the data in Fig. 3, but additional factors must be considered as the identity of the active oxides changes. Yet, many studies have proposed a persistent correlation between propane reactivity and reducibility in H_2 (16–21), without including the subtleties described above and without reporting *turnover* rates (per exposed MO_x) or *initial* (*low conversion*) reduction rates in H_2. Next, we show that a more fundamental relationship appears to exist between the rate of propane turnover and the ligand-to-metal electron transfer processes responsible for the near-edge region absorption features in the electronic spectra of dispersed metal oxides.

Diffuse reflectance UV–visible spectra were measured for VO_x, MoO_x, NbO_x, and WO_x domains supported on Al_2O_3 at varying MO_x surface densities. These electronic spectra reflect the structure of valence and conduction bands in bulk solids and of the frontier atomic orbitals in oxide domains too small to be described by a continuum spectrum of energy states. In both bulk and dispersed oxides, the bands arising from electronic transitions in the visible and UV energy range are typically broad, making their interpretation and assignment to specific structures difficult. The absorption edge energy, however, can be measured rigorously, and it provides an accurate description of the electronic properties of metal oxides (30), because it corresponds to incipient ligand-to-metal charge transfer processes in these materials.

Absorption edge energies were calculated using Tauc's law (25, 31). The absorption edge is defined by convention as the x-intercept of a linearized near-edge region for $[F(R_\infty)h\nu]^{1/2}$ as a function of $h\nu$, where $F(R_\infty)$ is the Kubelka–Munk function [28] and $h\nu$ is the energy of the incident photon. This form accurately describes the near-edge region for indirect band gap semiconductors and for amorphous semiconductors, such as those consisting of small oxide domains, irrespective of the charge-transfer mechanism. The absorption-edge energies estimated in this manner for all Al_2O_3-supported VO_x and MoO_x catalysts are shown in Fig. 5. Figure 5 shows that absorption-edge energies decrease with increasing VO_x or MoO_x surface density, suggesting that the energy required to promote an electron from the highest occupied molecular orbital (HOMO) in a lattice oxygen atom to the lowest unoccupied molecular orbital (LUMO) in the metal cation decreases as the surface density and the size of the two-dimensional active oxide domains increase. These results are consistent with similar trends reported earlier for dispersed MoO_x and WO_x

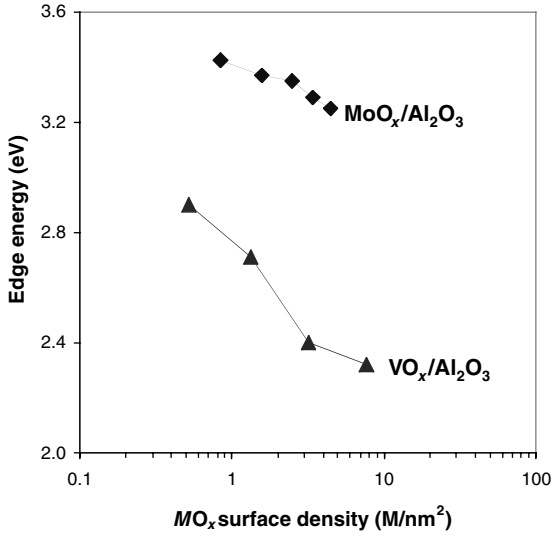

FIG. 5. Dependence of the UV–visible absorption edge energy on the MO_x surface density.

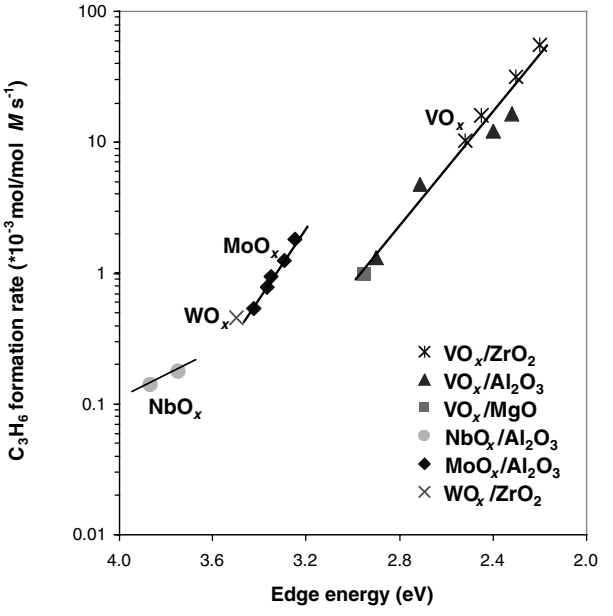

FIG. 7. Dependence of initial propene formation rate (703 K, 14 kPa C_3H_8, 1.7 kPa O_2, balance He) on the UV–visible absorption-edge energy for MO_x catalysts.

catalysts (24, 25, 30). At a given surface density, however, absorption energies are significantly higher for MoO_x than for VO_x samples. Next, we examine a possible relation between the ability of these materials to undergo oxygen-to-metal electronic transitions and their effectiveness in forming vacancies during propane ODH and during reduction with H_2.

Figure 6 shows the relationship between propane conversion turnover rates (plotted logarithmically) and UV–visible absorption-edge energies for VO_x, MoO_x, WO_x, and NbO_x domains supported on Al_2O_3, ZrO_2, or MgO. Turnover rates increase monotonically with decreasing absorption-edge energy, almost irrespective of the chemical identity of the active oxide. The turnover rates for propane conversion shown in Fig. 6 include both primary propane oxidative dehydrogenation and primary propane combustion reactions. On these materials, initial propene selectivities are very high (>80%); therefore, the trends detected in Fig. 6 for total propane conversion persist when propene formation rates are used instead (Fig. 7). As in the case of total rates, propene formation rates increase as the absorption-edge energies of the active oxide domains decrease. The observed correlation suggests that electron promotion processes responsible for the absorption edge involved in the kinetically relevant C–H bond activation share some common requirements with the photoexcitation process responsible for the absorption edge in all oxide domains examined (VO_x, MoO_x, NbO_x, and WO_x).

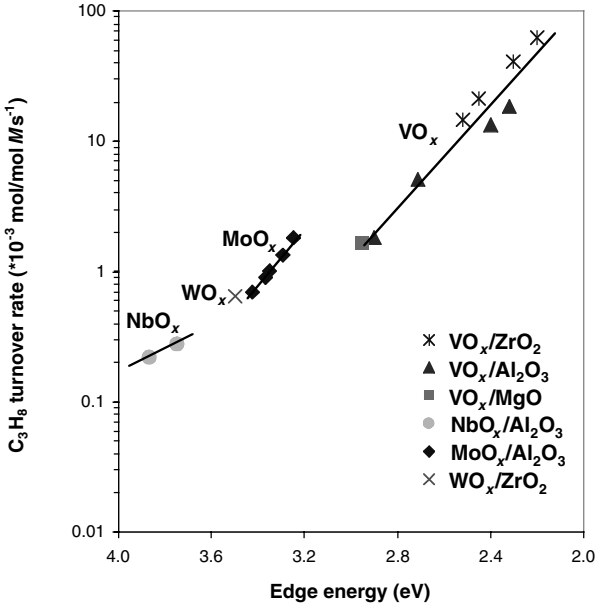

FIG. 6. Dependence of propane turnover rate (703 K, 14 kPa C_3H_8, 1.7 kPa O_2, balance He) on the UV–visible absorption edge energy for MO_x catalysts.

A discussion of these common features requires that we examine the details of propane ODH reactions on these active oxides. Propane turnover rates on VO_x and MoO_x domains are controlled by the dissociation of the first methylene C–H bond in propane. The transition state for this elementary step lies along a reaction coordinate in which two electrons are transferred from lattice oxygens to metal centers as an isopropoxide and a hydroxyl group form from propane (9–11). A plausible sequence, supported by molecular simulations (32) and consistent with kinetic and isotopic tracer measurements (9, 33), is shown in Fig. 8. The

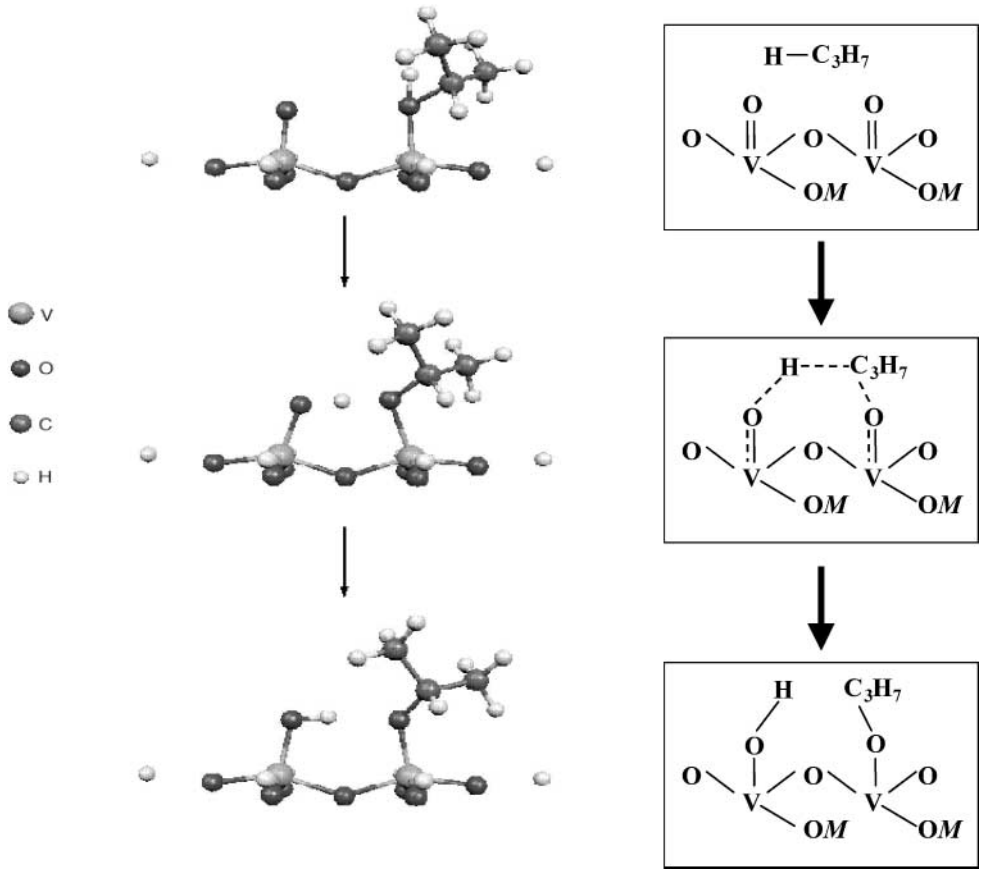

FIG. 8. Simulated example of C–H bond activation of propane using catalyst lattice oxygen.

methylene C–H bond in a propane molecule first interacts with lattice oxygen as a propane molecule adsorbs weakly on the oxide surface. The adsorbed propane reacts with a vicinal lattice oxygen atom to form an isopropoxide species and an OH group. The complete sequence of elementary steps required for an oxidative dehydrogenation turnover, confirmed previously by kinetic and isotopic tracer studies (9, 11), is shown in Fig. 9, where k_j denotes rate constants for irreversible steps and K_j equilibrium constants for quasiequilibrated steps.

Two lattice oxygen atoms ultimately become involved in the C–H activation step, and each one returns one electron to either a single metal center, leading to a two-electron reduction (e.g., V^{5+} to V^{3+}), or to two metal centers, each of which undergoes a one-electron reduction (e.g., V^{+5} to V^{+4}). These two processes require different energies, and the reaction will preferentially follow the path with the lower activation barrier. Molecular simulations (32) suggest that propane ODH reactions involve one-electron reduction of two V^{+5} centers to V^{+4} using one electron from each of two lattice oxygens, a process that requires a lower activation energy than a V^{5+}- to-V^{3+} reduction. The need for two V atoms to accommodate the transition state and the products in the rate-determining step may account for the low ODH turnover rates observed on small oxide domains (12, 13), such as monovanadate structures, which must undergo less favorable two-electron reduction of individual V atoms during each ODH catalytic turnover. Two or

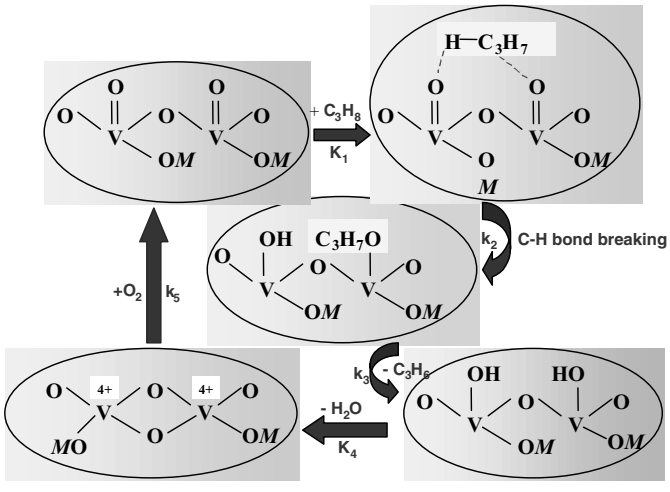

FIG. 9. Simulated example of propane oxidative dehydrogenation over VO_x-based catalyst.

more adjacent V and Mo sites appear to be required for other catalytic oxidation reactions (34, 35), and a sharp break in catalytic behavior is reported between monomer and oligomers of metal oxides. In the present study, the changes in catalytic behavior are much more gradual (12–15), because these samples do not exhibit sharp transitions in structure (e.g., from monovanadate to polyvanadate) with increasing surface density of the active oxide.

The transition state for propane activation during ODH reactions contains incipiently cleaved C–H and V–O bonds and partially formed O–C and O–H bonds. (Figs. 8 and 9) Molecular simulations and the empirical correlation between the rates of H_2 reduction and propane ODH both suggest that the required transition states for both processes involve electron transfer from lattice oxygen atoms to metal centers. The number of electrons transferred in the process of forming this activated complex must lie between zero (as in the reactants) and two (as in the products), because this elementary step lies along a reaction coordinate in which two V–O bonds are cleaved and O–C and O–H bonds are concurrently formed. Hammond's postulate states that transition states become increasingly productlike as an elementary step becomes less thermodynamically favorable. Therefore, as the breaking of metal–oxygen bonds becomes more difficult (e.g., as the cation changes from V to Mo to Nb), the reduced character of the cations in the transition state should increase, and the energy of formation of the transition state will respond more sensitively to the ability of each cation to accept electrons. In other words, as the energetics of the C–H bond activation state become less favorable, the activated complex increasingly resembles the reaction products. The stability of this transition state, and therefore the activation energy for C–H bond activation steps, depends on the energy required to transfer the required electrons from the oxygen ligands to the metal centers in a metal oxide. This energy determines also, in the case of excitation by photons, the energy at which absorption occurs in the UV–visible spectrum. As these electronic transitions require higher energies, either because of a decrease in oxide domain size or a change in the chemical identity of the oxide, propane ODH turnover rates concurrently decrease, as shown by the data presented in Figs. 6 and 7.

If all metal oxides shown in Figs. 6 and 7 followed the one-electron reduction path suggested for VO_x, a single general correlation would be expected. This is not supported by the data in Figs. 6 and 7. For all oxides, propane conversion turnover rates increase monotonically with decreasing absorption-edge energy, but the data for the different oxides are shifted slightly relative to each other. Also, the sensitivity of the rates to the absorption energy is weaker for VO_x domains than for MoO_x domains. Of course, the transition state structures suggested by the scheme in Fig. 8 include not only partially cleaved metal–oxygen bonds, but also the incipient formation of *M*–O–C and *M*–O–H bonds. The extent to which this evolution of chemical bonds has progressed at the point of maximum energy along the reaction coordinate (i.e., at the transition state) will depend on the relative energies of these various bonds and on whether the process involves one- or two-electron reduction of metal centers. Thus, although the edge energy is important for these materials to stabilize the required activated complexes, the extent to which it influences these reaction rates varies slightly as we change the identity of the metal oxide and the consequent finer details of the electron transfer processes involved.

As a comparison, Fig. 10 shows the relationship between H_2 reduction rates (in a logarithmic axis) and UV–visible absorption-edge energies for some VO_x and MoO_x samples supported on Al_2O_3 and ZrO_2. A decrease in absorption-edge energy leads to an increase in H_2 rates for VO_x and MoO_x supported on Al_2O_3 with varying surface density and domain sizes, but no clear general relationship emerges from the complete set of data shown in Fig. 10. These findings are in contrast to the more consistent relation found between ODH turnover rates and absorption energies. Clearly, the marked differences in structural or chemical properties of VO_x and MoO_x domains are "felt" differently by H_2 reduction and propane ODH reactions. While ODH reaction pathways are relatively well established (9–11), detailed H_2 reduction mechanisms remain unclear (22) and they emphasize the nucleation and growth processes that limit stoichiometric reductions leading to changes in crystal structure and not the chemistry of the H–H bond

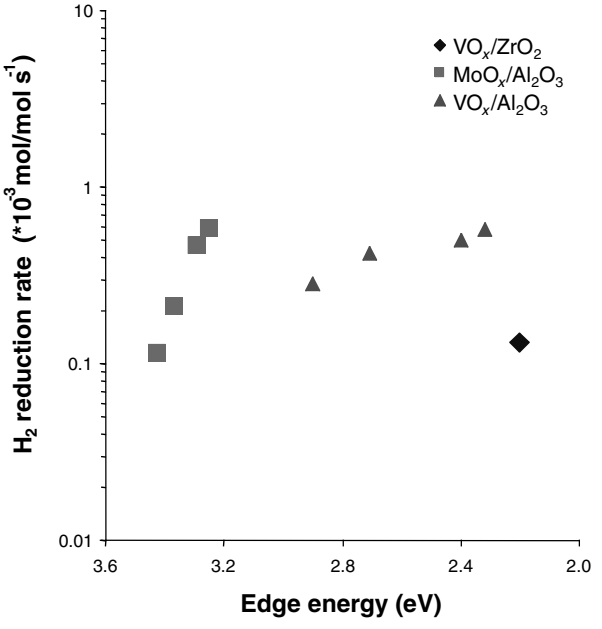

FIG. 10. Dependence of H_2 reduction rate (673 K, 20 kPa H_2, balance Ar) on the UV–visible absorption edge energy for MO_x catalysts.

activation and OH formation steps. In fact, one of the possible H_2 reduction pathways on transition metal oxides may include H_2 dissociation on a few active metal centers and hydrogen spillover to vicinal reducible oxides (22, 23), rendering this H_2 reduction process mechanistically unrelated to the redox cycles required for alkane ODH (9–11). Thus, the relationship between the tendency of oxides to reduce in H_2 and their ability to undergo fast redox cycles during ODH reactions remains tenuous. It is clearly less appropriate as a predictive tool as the identity of the oxide varies than as changes in the size and structure of domains occur for a given metal oxide.

CONCLUSION

Turnover rates for propane oxidative dehydrogenation increase in parallel with an increase in the rate of H_2 reduction and with a decrease in the UV–visible absorption-edge energies for supported two-dimensional transition metal oxides (VO_x, MoO_x, WO_x, and NbO_x). For a given metal oxide, propane conversion turnover rates increase as the rate of reduction in H_2 increases, suggesting the involvement of redox cycles in propane ODH kinetically relevant steps. For samples with similar H_2 reduction rates, V-based catalysts are much more active than Mo-based catalysts. Irrespective of the nature of the active oxide, propane turnover rates increase monotonically as the UV–visible absorption-edge energy decreases for all samples examined. For each of the oxides examined (VO_x, MoO_x, NbO_x, and WO_x) lower absorption energies correspond to higher propane turnover rates. These results combined with an analysis of the catalyst electron-transfer mechanism suggest that C–H bond dissociation proceeds via transition states requiring electron transfer from oxygen atoms to metal centers. The activation energy for this step appears to depend sensitively on energy required for electronic transitions responsible for the absorption edge in the UV–visible spectrum. As this transition occurs at lower energies, propane ODH turnover rates increase.

ACKNOWLEDGMENTS

This work was supported by the Director, Office of Basic Energy Sciences, Chemical Sciences Division, U.S. Department of Energy under Contract DE-AC03-76SF00098. The authors express their thanks to Varian Corp. for the donation of the UV–visible spectrophotometer to the Berkeley Catalysis Center. The authors acknowledge Dr. Chelsey Baertsch for the preparation of Nb- and W-based samples and Dr. Chanho Pak for the preparation of VO_x/MgO samples. The authors also thank Morris D. Argyle for insightful technical discussions.

REFERENCES

1. Blasko, T., and López Nieto, J. M., *Appl. Catal. A* **157**, 117 (1997).
2. Kung, H. H., *Adv. Catal.* **40**, 1 (1994).
3. Albonetti, S., Cavani, F., and Trifiro, F., *Catal. Rev.–Sci. Eng.* **38**, 413 (1996).
4. Centi, G., and Triffiro, F., *Appl. Catal. A* **143**, 3 (1996).
5. Mamedov, E. A., and Cortés-Corberan, V., *Appl. Catal. A* **127**, 1 (1995).
6. Meunier, F. C., Yasmeen, A., and Ross, J. R. H., *Catal. Today* **37**, 33 (1997).
7. Cadus, L. E., Gomez, M. F., and Abello, M. C., *Catal. Lett.* **43**, 229 (1997).
8. Lee, K. H., Yoon, Y. S., Ueda, W., and Moro-oka, Y., *Catal. Lett.* **46**, 267 (1997).
9. Chen, K., Khodakov, A., Yang, J., Bell, A. T., and Iglesia, E., *J. Catal.* **186**, 325 (1999).
10. Chen, K., Bell, A. T., and Iglesia, E., *J. Phys. Chem. B* **104**, 1292 (2000).
11. Chen, K., Iglesia, E., and Bell, A. T., *J. Phys. Chem. B* **105**, 646 (2001).
12. Khodakov, A., Olthof, B., Bell, A. T., and Iglesia, E., *J. Catal.* **181**, 205 (1999).
13. Khodakov, A., Yang, J., Su, S., Iglesia, E., and Bell, A. T., *J. Catal.* **177**, 343 (1998).
14. Chen, K., Xie, S., Bell, A. T., and Iglesia, E., *J. Catal.* **198**, 232 (2001).
15. Chen, K., Xie, S., Bell, A. T., and Iglesia, E., *J. Catal.* **195**, 244 (2000).
16. López Nieto, J. M., Soler, J., Concepción, P., Herguido, J., Menéndez, M., and Santamaría, J., *J. Catal.* **185**, 324 (1999).
17. Arene, F., Frusteri, F., and Parmaliana, A., *Catal. Lett.* **60**, 59 (1999).
18. Albrecht, S., Wendt, G., Lippold, G., Adamski, A., and Dyrek, K., *Solid State Ionics* **101**, 909 (1997).
19. Blasco, T., Galli, A., López Nieto, J. M., and Trifiró, F., *J. Catal.* **169**, 203 (1997).
20. Abello, M. C., Gomez, M. F., and Cadus, L. E., *Catal. Lett.* **53**, 185 (1998).
21. Grabowski, R., Grzybowska, B., Samson, K., Sloczynski, J., Stoch, J., and Wcislo, K., *Appl. Catal. A* **125**, 129 (1995).
22. Regalbuto, J. R., and Ha, J. W., *Catal. Lett.* **29**, 189 (1994).
23. Bosch, B. H., Kip, B. J., van Ommen, J. G., and Gellings, P. J., *J. Chem. Soc. Faraday Trans. 1* **80**, 2479 (1984).
24. Barton, D. G., Soled, S. L., Meitzner, G. D., Fuentes, G. A., and Iglesia, E., *J. Catal.* **181**, 57 (1999).
25. Barton, D. G., Shtein, M., Wilon, R. D., Soled, S. L., and Iglesia, E., *J. Phys. Chem. B* **103**, 630 (1999).
26. Pak, C., Bell, A. T., and Tilley, T. D., *J. Catal.* **206**, 49 (2002).
27. Baertsch, C., Ph.D. dissertation, University of California at Berkeley, 2001.
28. Delgass, W. N., "Spectroscopy in Heterogeneous Catalysis." Academic Press, New York, 1979.
29. Chen, K., Bell, A. T., and Iglesia, E., unpublished results.
30. Weber, R. S., *J. Catal.* **151**, 470 (1995).
31. Tauc, J., *in* "Amorphous and Liquid Semiconductors" (J. Tauc, Ed.). Plenum, London, 1974.
32. Gilardoni, F., Bell, A. T., Chakraborty, A., and Boulet, P., *J. Phys. Chem. B* **104**, 12250 (2000).
33. Chen, K., Iglesia, E., and Bell, A. T., *J. Catal.* **192**, 197 (2000).
34. Racine, B. N., Sorensen, C. M., and Weber, R. S., *J. Catal.* **142**, 735 (1993).
35. Neumann, R., and Levin, M., *J. Am. Chem. Soc.* **114**, 7278 (1992).